

DANCE: Dynamic 3D CNN Pruning: Joint Frame, Channel, and Feature Adaptation for Energy Efficiency on the Edge

Mohamed Mejri Ashiqur Rasul Abhijit Chatterjee

School of Electrical and Computer Engineering, Georgia Tech, Atlanta, GA, USA

mmejri3@gatech.edu, arasul6@gatech.edu, abhijit.chatterjee@ece.gatech.edu

Abstract

Modern convolutional neural networks (CNNs) are workhorses for video and image processing, but fail to adapt to the computational complexity of input samples in a dynamic manner to minimize energy consumption. In this research, we propose DANCE, a fine-grained, input-aware, dynamic pruning framework for 3D CNNs to maximize power efficiency with negligible to zero impact on performance. In the proposed two-step approach, the first step is called activation variability amplification (AVA) and the 3D CNN model is retrained to increase the variance of the magnitude of neuron activations across the network in this step, facilitating pruning decisions across diverse CNN input scenarios. In the second step, called adaptive activation pruning (AAP), a lightweight activation controller network is trained to dynamically prune frames, channels and features of 3D convolutional layers of the network (different for each layer), based on statistics of the outputs of the first layer of the network. Our method achieves substantial savings in multiply-accumulate (MAC) operations and memory accesses by introducing sparsity within convolutional layers. Hardware validation on the NVIDIA Jetson Nano GPU and the Qualcomm Snapdragon 8 Gen 1 platform demonstrates respective speedups of $1.37\times$ and $2.22\times$, achieving up to $1.47\times$ higher energy efficiency compared to the state of the art.

neural networks are computationally expensive, with costs that grow with network depth and scaling from 2D (image [27, 31]) to 3D (video or point cloud [33, 38]) processing. To address this, structured pruning has emerged as a promising solution [5, 9, 19, 20], reducing both memory footprint and computational requirements. Pruning can also be applied dynamically, removing parameters adaptively depending on the input [4, 7, 12, 22, 26, 35, 40]. Despite the fact that dynamic pruning has been applied mostly to 2D CNNs, where focus is largely on coarse strategies such as channel pruning or layer removal techniques, which, while effective, remain limited in granularity and overall scope of power efficiency.

In this work, we propose DANCE, a two-step, fine-grained, input-aware pruning framework for 3D convolutional neural networks that dynamically removes unnecessary frames, channels, and features inside intermediate 4D ($height \times width \times channel \times frame$) activation tensors of the hidden layers of the network. The first step, referred to as *activation variability amplification (AVA)*, consists of training the network while increasing the variance of activation magnitudes across the frames, channels, and features inside the network. This variance amplification facilitates later pruning by reinforcing critical neurons and suppressing redundant neurons. The second step, *adaptive activation pruning (AAP)*, introduces a lightweight *activation controller network* that dynamically prunes frames, channels, and features corresponding to different hidden layers of the network for each input sample, based on thresholds applied to the aggregated outputs (representing statistics) of the first layer of the network. This enables the 3D CNN model to skip unnecessary neurons dynamically, allowing each input sample to trigger a tailored pruning pattern across the frames, channels, and features of each hidden layer. Computational savings arise from skipping operations tied to pruned activations, greatly reducing MAC operations and memory accesses. Additionally, removing noisy or irrelevant activations can enhance accuracy by filtering out noisy or misleading features. *The sparsity of channels and feature activations varies both from frame*

1. Introduction

Convolutional neural networks (CNNs) are widely used for computer vision applications involving both 3D and 2D structures, such as for videos and images, respectively, for tasks such as gesture classification, action recognition, video caption generation, object detection and tracking, semantic segmentation and so on. However, convolutional

¹Code and experimental data of this research work will be published after acceptance of the article.

to frame and across different convolutional layers in a 3D CNN. The key contributions of this paper are:

(1) We propose a novel *input-aware adaptive fine-grained pruning framework* for 3D convolutional neural networks, capable of dynamically pruning frames, channels, and features in 4D activation tensors of the hidden layers of the network, on a per-layer basis, based on statistics of the outputs of the first layer of the network.

(2) A *two-step adaptation process* is used: (1) **Activation variability amplification (AVA)**, which increases activation variance across the 4D activation tensor dimensions, without degrading network performance, and (2) **Adaptive activation pruning (AAP)**, which employs a lightweight network to predict input-aware pruning thresholds for frame, channel, and feature pruning, allowing each input sample to trigger a tailored pruning pattern.

(3) The proposed method introduces structured sparsity to reduce compute and memory overhead while maintaining (and sometimes improving) accuracy compared to prior work. We demonstrate the versatility of our approach on an NVIDIA Jetson Nano GPU and a Snapdragon 8 Gen 1 (Samsung S22) mobile CPU. By leveraging custom Neon SIMD kernels, we have achieved computational speedups of $1.37\times$ and $2.22\times$, respectively, with up to $1.47\times$ higher energy efficiency over optimized baselines.

2. Related Works

To develop input adaptive neural networks with dynamic computational graphs, researchers have approached the problem from three angles: sample-wise adaptive, spatially adaptive, and temporally adaptive. Sample-wise adaptive models adapt their computational graphs according to the complexity of individual input instances, whereas spatially adaptive and temporally adaptive neural networks modify and optimize themselves along spatial and temporal dimensions. Layer and channel skipping[26, 35, 40] is a popular technique to avoid unnecessary computation in neural networks, and this method involves adopting gating or halting mechanisms using an auxiliary policy network. BlockDrop[39] suggested a policy gradient reinforcement learning (REINFORCE)[11, 36, 44] algorithm for block selection within residual neural network architectures. The authors of Conditional Deep Learning [26] propose to add linear classification heads at the end of each convolution block, creating a cascaded architecture for early exit neural networks. Class-aware channel pruning [1, 14] methods dynamically reduce the model computational burden by selecting the important kernels based on class-aware saliency scores. Furthermore, a unified static and dynamic pruning framework has been suggested in the works of [6] with differentiable gating and channel selection mechanism using the Gumbel [13, 21] sigmoid trick. Aforementioned optimization techniques can be extended to 3D convolutional

neural networks for efficient processing of their relatively demanding computational task as well. Few research works have been conducted on static compression and pruning of 3D neural networks [25, 41], however, most of the investigations lack the essence of adaptation in their performance optimization scheme. Li et al [18] formulated an adaptive policy to optimize the use of 3D convolutional kernels where a reinforcement learning based selection network governs the usage of frame and convolutional filters. Additionally, Chen et al [3] proposed a pruning technique on the basis of converting convolutional kernels in the temporal axis to frequency domain representations, reducing the computational complexity by removing insignificant frequency components.

3. Overview

The framework for the proposed dynamic 3D CNN pruning approach is given in Figure 1. Figure 1 (top) shows input frames (video) to our system that are processed by the first convolutional layer (3D Conv 1) of the network. The outputs of the first layer are passed to an *Adaptive Activation Pruning (AAP) Controller* module. The AAP controller generates control signals for the active pruning of frames, channels, and features of all subsequent 3D convolutional layers in the network, as described below.

An expanded view of the “3D Conv 4” layer is shown in Figure 1, serving as the reference structure for all subsequent layers throughout the network. The inputs to this layer consist of C_{in} channels, with each $H \times W$ feature map corresponding to the respective channel filter, replicated over T temporal frames of video input, forming a 4D tensor as illustrated in box 1. Box (2) of Figure 1 shows the unfolded “flattened” representation (matrix) of the 4D tensor above. The rows and columns of this matrix are modulated by the AAP controller as shown in box (3) of Figure 1. Frame pruning eliminates one or more complete frames of the matrix ($H_i \times W_i$ rows, $1 \leq i \leq T$, box (3) top). Channel pruning eliminates complete columns of the matrix, while feature pruning eliminates corresponding weights of feature maps across all the channels of the network corresponding to different time frames (different for different time frames). The rearranged tensor is shown in box (4) of Figure 1. The pruned tensor is subsequently convolved with the kernels of the current layer, 3D Conv 4, to produce the output, shown as the 4D tensor in box (5), which serves as the input to the next layer in the network. Computational savings are achieved during convolution by skipping the operations associated with pruned frames, channels, and features. Based on the framework described in Figure 1 the dynamic pruning approach proceeds in two steps.

Step (1): To facilitate dynamic pruning it is necessary to amplify the effects of diverse network inputs (video frames across time, images) on the outputs of all the layers of the

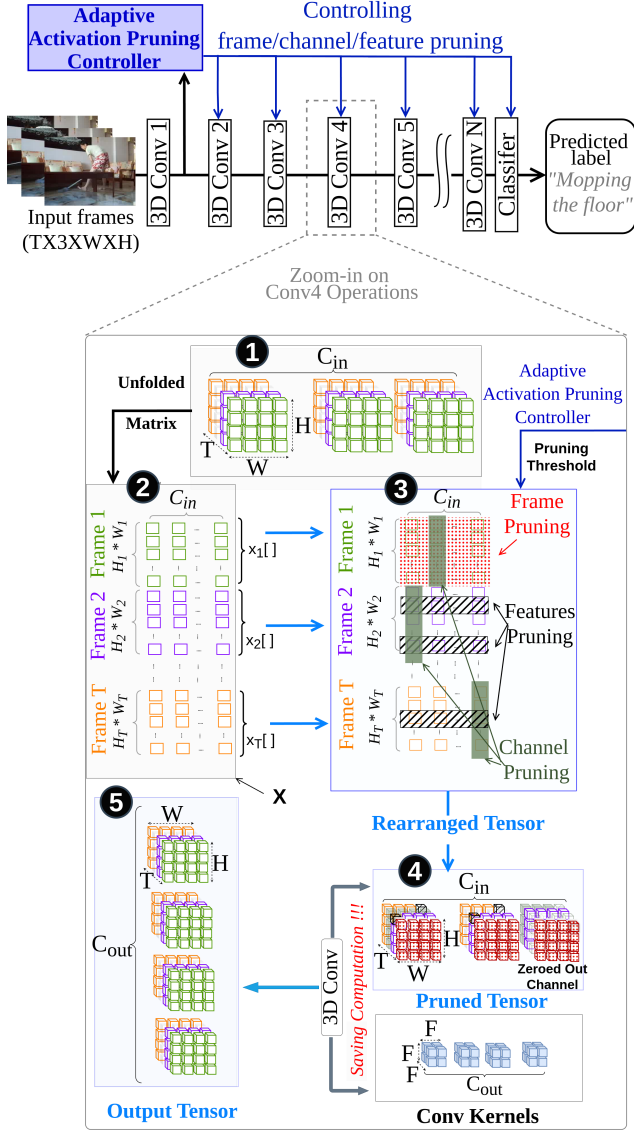


Figure 1. Illustration of 4D tensor pruning in intermediate convolution layers. Sparsity in the activation tensor is introduced at three levels by dynamic pruning: for frames (dotted in red), channels (shaded in green), and features (lined in black and white).

3D convolution network of Figure 1. A novel 3D CNN training method called *activation variability amplification* (AVA) is used to increase the variance of the distributions of the magnitudes of neuron activations across frames, channels, and features of the layers of the network of Figure 1. After model training, the post-AVA magnitude distribution exhibits higher variation across all corresponding 4D tensor dimensions. This induced variation enables clearer separation between relevant and irrelevant frames, channels, and features for more effective dynamic pruning.

Step (2): The outputs of the first layer of the network are passed to an adaptive activation pruning (AAP) controller

module. This eliminates frames, channels, and features of individual layers of the network based on processing of the outputs of the first layer and a generated threshold for each pruned element (inspired by the component retention criterion in Principal Component Analysis (PCA)[23], adapted here to operate on activation magnitudes as described in Step 1). It is worth mentioning that, only the parameters involved in the adaptive activation pruning controller are learned in the second step (refer to figure 1), while other parameters are kept frozen. In the following, Steps (1) and (2) are discussed in Sections 4 and 5, respectively.

4. Activation Variability Amplification (AVA)

Figure 2 describes the proposed **adaptive variability amplification** (AVA) training procedure of Step 1 discussed in Section 3. Inspired by the Convolutional Block Attention Module (CBAM) [37], which enhances the representational power of 2D convolutional neural networks through channel and features attention, the AVA module extends this concept by applying three hierarchical attention modules: frame, channel, and feature based attention. Unlike CBAM, our approach serves a different purpose: to quantify and adaptively re-weight neuron activation variability across the frame, channel, and feature dimensions. These attention modules help reweighting frames, channels and features within the activation tensor which helps increasing their magnitude variability.

Frame Attention Module: Consider the “flattened” 4D tensor X shown in Box (2) of Figure 1. This is also interchangeably represented as a matrix $X[]$, with sub-matrices $[x_1[], x_2[], \dots, x_T[]]$. Each sub-matrix $x_t[j, k]$ is of dimension $H_t * W_t$ by C_{in} (rows by columns) corresponding to each frame t , $1 \leq t \leq T$, as shown in the figure. Consider a trainable vector W_{FR} of dimension T , $W_{FR} = [w_{FR}(1), w_{FR}(2), \dots, w_{FR}(T)]$. If we assume that H_t is equal to a fixed height H and W_t is equal to a fixed width W for all $1 \leq t \leq T$, we compute:

$$L_{FR}(t) = \frac{|w_{FR}(t)|}{C \cdot H \cdot W} \sum_{j=1}^{H*W} \sum_{k=1}^C |x_t[j, k]| \quad (1)$$

The variance of $L_{FR}(t)$ over all $1 \leq t \leq T$ is denoted as σ_{FR}^2 . Maximizing σ_{FR}^2 during training helps in determining the relevance of different frames relative to others on a per-input basis. The sub-matrices $x_t[], 1 \leq t \leq T$ are weighted by the scalars $w_{FR}(t)$ (represented in tensor form as $X_{FR} = \text{ReLU}(X * W_{FR})$ in Figure 2) and passed on to the channel attention module.

Channel Attention Module: The weighted matrices $x'_t[j, k] = \text{ReLU}(w_{FR}(t) * x_t[j, k]), 1 \leq t \leq T$, are forwarded to a channel attention module, where channel-wise modulation is performed using the trainable vector $W_{CH} = [w_{CH}(1), w_{CH}(2), \dots, w_{CH}(C_{in})]$. A frame-dependent, channel-wise quantity $L_{CH}(t, c), 1 \leq t \leq T$,

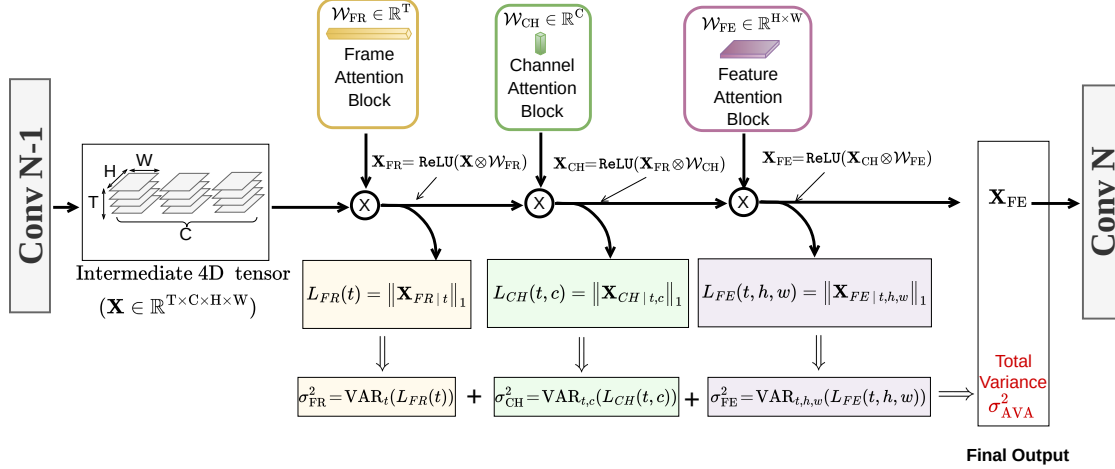


Figure 2. Overview of the Activation Variability Amplification (AVA) mechanism. Variance along the frame (L_{FR}), channel (L_{CH}) and feature (L_{FE}) dimensions are aggregated to determine the total variance σ_{AVA}^2 , which is used as parameter in the loss function to train the model for boosting variance within activations.

$1 \leq c \leq C_{in}$, is computed as:

$$L_{CH}(t, c) = \frac{|w_{CH}(c)|}{H \cdot W} \sum_{j=1}^{H \cdot W} |x'_t[j, c]| \quad (2)$$

The variance of $L_{CH}(t, c)$ over all $1 \leq t \leq T$, $1 \leq c \leq C_{in}$, is computed as σ_{CH}^2 . Maximizing σ_{CH}^2 during training helps in determining the relevance of different channels relative to others on a per-input basis. The tensor X_{CH} depicted by the columns of the sub-matrices $x'_t[\cdot]$ (representing channels), weighted by the scalars $w_{CH}(c)$, $1 \leq t \leq T$, $1 \leq c \leq C_{in}$, given as $X_{CH} = \text{ReLU}(X_{FR} \times W_{CH})$ in Figure 2 are passed on to the feature attention module.

Feature Attention Module: The columns of the sub-matrices $x'_t[j, k]$ above, are weighted by the quantities $w_{CH}(k)$, $1 \leq k \leq C_{in}$, to yield the sub-matrices $x^*_t[j, k]$. These are forwarded to a feature attention module where feature-wise modulation is performed using the trainable parameter $W_{FE} = [w_{FE}(1), w_{FE}(2), \dots, w_{FE}(H \cdot W)]$. A frame-dependent feature-based quantity L_{FE} is derived as follows:

$$L_{FE}(t, f) = \frac{|w_{FE}(f)|}{C} \sum_{c=1}^C |x^*_t[f, c]|, \quad (3)$$

where f is a row index for the sub-matrix $x^*_t[\cdot]$, $1 \leq f \leq H \cdot W$. The variance of $L_{FE}(t, f)$ over all $1 \leq t \leq T$, $1 \leq f \leq H \cdot W$, is computed as σ_{FE}^2 . Maximizing σ_{FE}^2 during training helps in determining the relevance of different features relative to others on a per-input basis. The tensor X_{FE} depicted by the rows of the sub-matrices $x^*_t[\cdot]$ (representing features), weighted by the scalars $w_{FE}(f)$, $1 \leq t \leq T$, $1 \leq f \leq H \cdot W$, given as $X_{FE} = \text{ReLU}(X_{CH} \times W_{FE})$

in Figure 2 are passed on to further convolutional layers of the network and for computation of the objective function for network training.

The frame, channel and feature based variances referred as σ_{FR}^2 , σ_{CH}^2 and σ_{FE}^2 respectively are aggregated to generate the total variance denoted σ_{AVA}^2 . The total variances from all the AVA modules inside the 3D CNN are summed together to generate the final variance referred to as σ_f^2 . The 3D CNN is then trained to jointly minimize the cross-entropy loss \mathcal{L}_{CE} between predicted and ground-truth labels and maximize the aggregated variance σ_{AVA}^2 . The overall objective function is defined as:

$$\mathcal{L}_f = \mathcal{L}_{CE} - \beta \sigma_f^2$$

where β is a small positive weighting factor that regulates the contribution of the variance term, ensuring that the optimization primarily focuses on reducing classification error while increasing feature variability.

The choice of the standard deviation also serves the purpose of sparsity maximization. In our setting, the quantities $L_{CH}(t, c)$, $L_{FE}(t, f)$, and $L_{FR}(t)$ are first normalized with respect to the ℓ_1 norm, i.e., their entries are nonnegative and rescaled to sum to one. Under this normalization, Lemma 1 shows that maximizing the standard deviation is equivalent to maximizing sparsity in the sense of the Hoyer measure [42], defined for a vector $\mathbf{x} \in \mathbb{R}^D$ as

$$H(\mathbf{x}) = \frac{\sqrt{D} - \frac{\|\mathbf{x}\|_1}{\|\mathbf{x}\|_2}}{\sqrt{D} - 1}.$$

Lemma 1. On the probability simplex Δ^{D-1} , the standard deviation $\text{std}(\mathbf{x})$ and the Hoyer measure $H(\mathbf{x})$ are

both strictly increasing functions of $\|\mathbf{x}\|_2$. Consequently, $\arg \max_{\mathbf{x} \in \Delta^{D-1}} \text{std}(\mathbf{x}) = \arg \max_{\mathbf{x} \in \Delta^{D-1}} H(\mathbf{x})$.

Proof. Since $\|\mathbf{x}\|_1 = 1$, then $\bar{x} = 1/D$ and $\text{std}(\mathbf{x})^2 = \frac{1}{D} \|\mathbf{x}\|_2^2 - \frac{1}{D^2}$, which is strictly increasing in $\|\mathbf{x}\|_2$. Similarly, for $\mathbf{x} \in \Delta^{D-1}$, the Hoyer measure simplifies to $H(\mathbf{x}) = \frac{\sqrt{D-1} \|\mathbf{x}\|_2}{\sqrt{D-1}}$. Because the term $-1/\|\mathbf{x}\|_2$ is strictly increasing in $\|\mathbf{x}\|_2$, $H(\mathbf{x})$ is also a strictly increasing function of $\|\mathbf{x}\|_2$. Since both objectives are monotonic transformations of the same norm, they share identical maximizers. \square

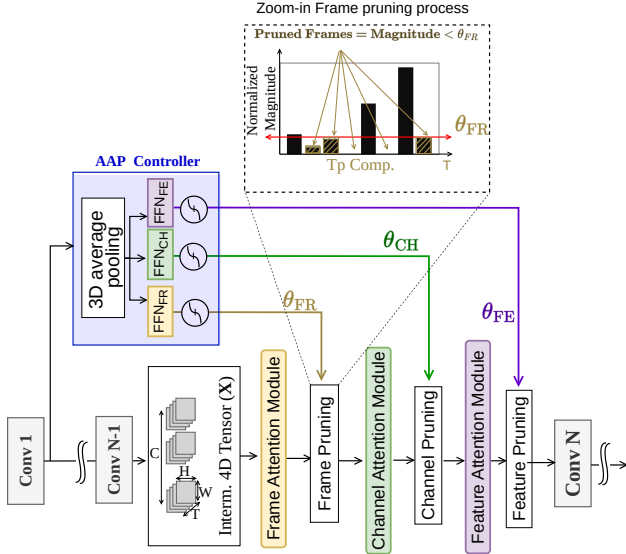


Figure 3. Adaptive Activation Pruning (AAP): The AAP function is applied sequentially on frames, channels, and features (depicted from top to bottom) to produce a structured sparsity pattern in the activation tensor fed into the subsequent convolutional layer.

5. Adaptive Activation Pruning (AAP)

Adaptive activation pruning (AAP) introduces sparsity into the activation tensors of intermediate convolutional layers of the network based on precomputed thresholds. Following the variability amplification phase, high variance within activation tensor dimensions stimulates large magnitude differences among frames, channels, and features, which in turn facilitates elimination of unnecessary frames, channels, and features (those with low magnitude) from the computation graph and following the step, the *weights of the 3D convolutional network are frozen and only the parameters of the AAP module are trained*. Figure 3 illustrates the processing involved in the Adaptive Activation Pruning (AAP) module, and proceeds in three consecutive steps.

The output of the 1st convolutional layer of the 3D CNN serves as input to the AAP controller, which utilizes 3D average pooling followed by three FFNs (FFN_{FR} , FFN_{CH} ,

FFN_{FE}) and sigmoid activations to produce global pruning thresholds θ_{FR} , θ_{CH} , and θ_{FE} . These thresholds are shared across all layers and operate within $[0, 1]$ due to the normalization of the importance metrics (L). While a global threshold may be less efficient than layer-wise adaptation, it avoids the linear overhead of per-layer modules, preserving the net computational benefit. Pruning is executed as follows: frames t are suppressed if $L_{\text{FR}}(t) \leq \theta_{\text{FR}}$ (Eq. 1), channels if $L_{\text{CH}}(t, c) \leq \theta_{\text{CH}}$ (Eq. 2), and features if $L_{\text{FE}}(t, c) \leq \theta_{\text{FE}}$ (Eq. 3).

As illustrated in Figure 3, frame, channel, and feature pruning are applied after each corresponding attention module to the intermediate 4D tensor (\mathbf{X}) using the retention thresholds described above.

Since the model has already been trained with the AVA module, retraining the entire network while pruning is unnecessary and could even reduce variability in intermediate activations. Therefore, the 3D CNN weights are kept frozen, and only the AAP controller network is trained to produce higher retention thresholds while maintaining classification performance.

However, training the AAP controller network jointly with adaptive activation pruning poses a challenge, as pruning involves non-differentiable binary mask generation. To address the non-differentiability issue, we adopt the Straight-Through Estimator (STE) technique [2], which applies a hard (non-differentiable) operation in the forward pass and a soft counterpart in the backward pass, allowing gradients to flow through the 3D CNN. For the binary mask generation, we employ a soft gating operation inspired by the Gumbel-Softmax technique [13, 21, 28], as shown in Equation 4:

$$y = \begin{cases} \mathbb{1} \left[\frac{x - \theta + n}{\tau} \geq 0 \right], & \text{(forward pass),} \\ \sigma \left(\frac{x - \theta + n}{\tau} \right), & \text{(backward pass).} \end{cases} \quad (4)$$

In Equation 4, σ represents the sigmoid function, x de-

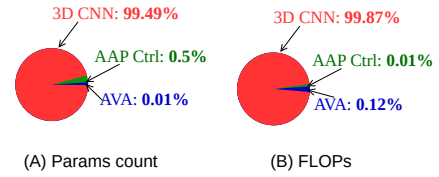


Figure 4. Overhead of the 3D CNN, AVA modules, and AAP controller

notes the normalized magnitude of frames, channels, or pixels; θ represents the retention threshold, and $n \sim \mathcal{N}(0, \epsilon)$ is a Gaussian noise term with zero mean and small variance ϵ , introduced to smooth the threshold boundary. This stochasticity enables more stable gradient flow near decision boundaries. The output y populates the binary mask

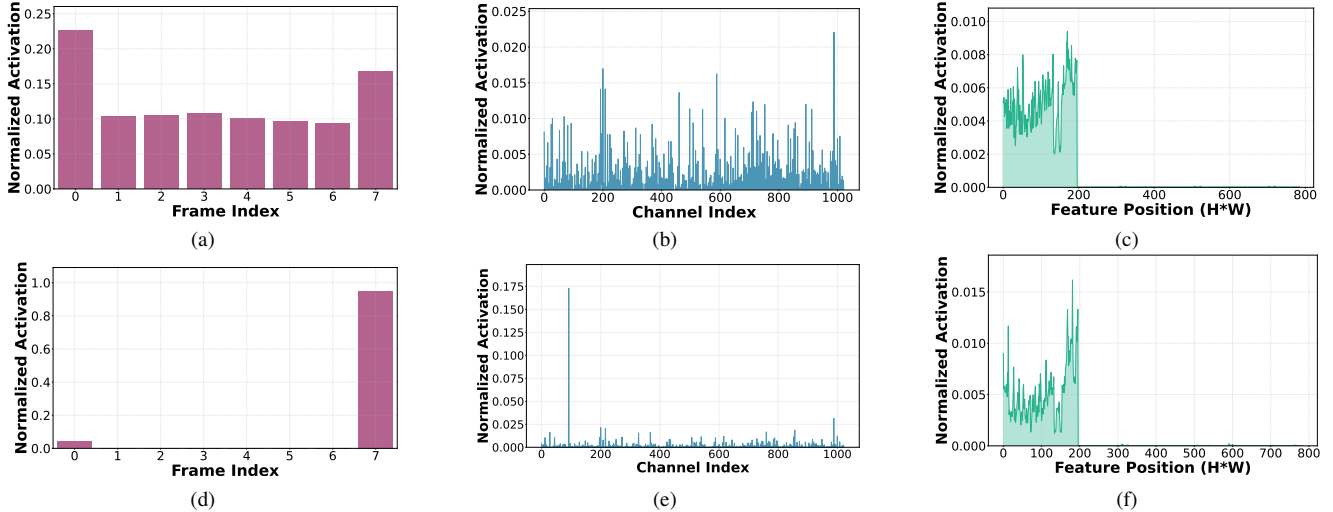


Figure 5. Visualization of frame, channel, and feature magnitude distribution before and after AVA

with 1 if the normalized magnitude is above the threshold and zero otherwise. The AAP controller network is trained to adaptively select the highest possible retention thresholds, resulting in higher pruning rates while maintaining accuracy. The final objective loss is thus defined as:

$$\mathcal{L}_f = \mathcal{L}_{CE} - \lambda \cdot \sum_{\theta \in \text{AAP Modules}} (\theta_{FR} + \theta_{CH} + \theta_{FE})$$

where λ is a small hyperparameter controlling the regularization strength.

6. Experimental Results

We first present simulation results for computational efficiency and final model accuracy after pruning on a baseline dataset, and compare the same against state-of-the-art methods. Next, we conduct an ablation study to assess (1) the importance of the AVA step and (2) the effect of retraining the full network together with the AAP controller on accuracy and pruning ratio. We then report the overhead introduced by the AAP controller and AVA modules relative to the 3D CNN model. Subsequently, we describe the pruning ratios for individual components; frames, channels, and features, and provide visual profiles of their magnitude distributions before and after the AVA procedure. We also include per-layer FLOP profiles before and after pruning. Finally, we show the speedup and energy efficiency achieved on validation hardware.

Tables 1 and 2 compare respectively, our method against state-of-the-art (SOTA) pruning schemes on UCF101 [30] and HMDB51 [16] using the R(2+1)D [34] and C3D [32] models pretrained on Kinetics [15], reporting pruning rates, baseline accuracies, and post-pruning top-1 accuracies. Across all settings, our dynamic, fine-grained pruning consistently outperforms existing static approaches. On

Model	Sparsity Scheme	Pruning Rate	Baseline Acc. (%)	Top-1 Acc. (%)	Δ Acc. (%)
R(2+1)D[34]	Filter	2.6 \times	94.5	90.5	-4.00
	Vanilla	2.6 \times		91.7	-2.80
	KGS[25]	3.2 \times		92.0	-2.50
	KGRC	3.02 \times		92.65	-1.85
	<i>Our method</i>	4.0\times	91.5	93.05	+1.55
C3D[32]	DCP[43]	1.99 \times	82.77	71.72	-11.05
	FP[17]	2.02 \times		75.44	-7.33
	TP[24]	2.02 \times		70.00	-12.77
	MDP[8]	2.00 \times		76.82	-5.95
	MDP+KD	2.00 \times		80.10	-2.67
		KGR		1.76 \times	81.84
	KGC	1.93 \times	82.82	81.39	-1.43
	KGRC	3.04 \times	80.21	-2.61	
	<i>Our method</i>	3.49\times	87.9	87.93	+0.03

Table 1. Comparison of pruning methods on UCF101.

Sparsity Scheme	Pruning Rate	Accuracy (%)	Δ Acc. (%)
DCP[43]	2.02 \times	40.59	-7.6
FP[17]	2.02 \times	40.98	-7.2
TP[24]	2.11 \times	34.84	-13.3
MDP[8]	2.14 \times	43.20	-4.9
MDP+KD	2.14 \times	45.62	-2.6
<i>Our method</i>	2.77\times	46.17	-2.02

Table 2. Performance comparison of model compression approaches on HMDB51 (Split 1), using pruning ratio and accuracy improvements over the C3D baseline.

UCF101 with R(2+1)D [34], we achieve a 4 \times pruning rate compared to the best SOTA technique, (which achieves 3.02 \times), while improving accuracy by 1.5%, whereas all static baselines incur accuracy degradation. For UCF101 with C3D [32], our method provides a 3.49 \times pruning rate—higher than the best SOTA at 3.04 \times , with no accuracy drop. On HMDB51 with C3D, we again surpass all prior work with a 2.77 \times pruning rate versus 2.14 \times , and only

a minimal 2% accuracy reduction. Overall, the tables show that dynamic pruning coupled with fine-grained sparsification yields more optimal compression and superior accuracy preservation than the coarse-grained static strategies used in current state-of-the-art methods. The higher baseline accuracies (91.5% for $R(2+1)D$ and 87.9% for $C3D$) result from the AVA module acting as a feature enhancer that strengthens representations by suppressing redundant activations. This dual-purpose design facilitates fine-grained pruning while simultaneously boosting model robustness, enabling superior compression rates without the accuracy degradation typical of SOTA methods.

Metric	UCF101			HMDB51		
	w/ AVA	w/o AVA	AAP Co-train	w/ AVA	w/o AVA	AAP Co-train
Pruning rate	3.49	1.1	2.86	2.77	1.2	2.32
Accuracy	87.93	85.04	86.7	46.17	44.5	45.57

Table 3. Ablation study on pruning rate and accuracy for UCF101 and HMDB51 with and without the AVA step.

Dataset	Frame only	Channel only	Feature only	Combined
UCF101	1.03×	2.47×	1.50×	3.49×
HMDB51	1.35×	2.62×	1.39×	2.77×

Table 4. Pruning-ratio distributions (frame, channel, feature, combined) for C3D on UCF101 and HMDB51.

Table 3 shows that AVA is essential; without it, uniform activation magnitudes prevent the AAP controller from establishing effective pruning thresholds. Furthermore, co-training the CNN and AAP controller disrupts the structured variability required for pruning, decreasing accuracy without providing additional overhead reduction.

Figure 4 further shows that both AVA and the AAP controller add negligible memory and computation relative to the main CNN, confirming that these components are necessary and introduce minimal overhead.

Table 4 shows how frame, channel, and feature pruning individually contribute to pruning the full C3D model on UCF101 and HMDB51 datasets. In both cases, channels are the sparsest component and provide over twice the overhead reduction of frames and features. Features exceed frames only in activation pruning, as removing a full frame would significantly degrade CNN accuracy.

As depicted in figure 5, variance is boosted along the frame, channel, and feature dimensions of the C3D model by suppressing the redundant neurons, and the sub-figures show the contrast in normalized activation magnitude at the fourth convolutional layer of the C3D model for a sample input. From our experiments, it has been observed that the adaptive variability amplification framework is more effective along the frame or channel dimension, compared to the feature. Training the model to increase variance within the activation tensor, therefore, facilitates the elimination of re-

dundant neurons, which in turn, promotes sparsity when passed through the Adaptive Activation Pruning module.

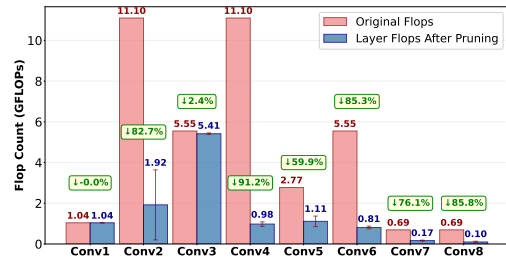


Figure 6. FLOPs reduction per conv. layer in the C3D model.

Figure 6 shows the average FLOP reduction across the C3D convolutional layers. Red bars indicate dense-layer FLOPs, while blue bars show FLOPs after introducing activation sparsity. The first layer shows no reduction because its output is needed by the AAP controller. From the second layer onward, sparsity has a clear impact. The red vertical lines denote each layer’s FLOP range, with Conv2 showing the greatest variation. Conv2 and Conv4 also achieve the largest pruning gains due to their high original computational overhead. Figure 7 illustrates the distribution of inference computational overhead (FLOPs) after adaptive pruning of the two baseline 3D CNN architectures: C3D (Figure 7a) and R2+1D (Figure 7b). The computational cost is analyzed with respect to the input information level of each video.

The spatial and temporal information measures, denoted as R^s and R^t , quantify the structural complexity within frames and the variability across frames, respectively. Inspired by the information-theoretic formulation in [29] and later used in [10], both metrics are derived from spatio-temporal DCT energy ratios between high- and low-frequency components and are log-normalized as $R = \log\left(1 + \frac{E_{\text{high}}}{E_{\text{low}}}\right)$ to stabilize variance and reduce skewness.

We model the relationship between intrinsic video information content and the computational effort required during inference. A strong correlation is observed between $[R^s, R^t]$ and FLOPs. For C3D, the multiple correlation coefficient and coefficient of determination are $R = 0.863$ and $R^2 = 0.745$, respectively, indicating that 74.5% of the vari-

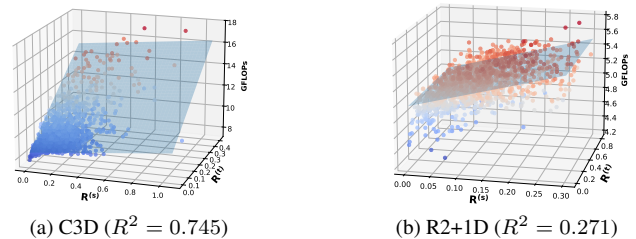
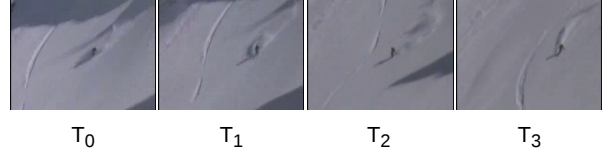


Figure 7. Inference GFLOPs distribution on UCF-101 for different adaptively pruned models w.r.t. spatial and temporal information



(a) Highest-complexity example: Rafting activity



(b) Lowest-complexity example: Skiing activity

Figure 8. Two extrema examples from UCF101 processed with C3D. The left video frames (Rafting) correspond to the maximum computational cost (14.5 GFLOPs), while the right video frames (Skiing) correspond to the minimum computational cost (7.8 GFLOPs).

ance is explained by input complexity. In contrast, R2+1D exhibits weaker correlation ($R = 0.521$, $R^2 = 0.271$).

These results confirm that the proposed adaptive framework is input-dependent, allocating more computation to videos that are more complex from an information-theoretic perspective. The disparity between C3D and R2+1D stems from architectural differences: R2+1D is a residual network in which skip connections limit the propagation of sparsity across layers, whereas C3D follows a VGG-style architecture without skip connections, allowing sparsity to accumulate and making its cost more sensitive to input complexity.

Figure 8 presents representative frames from the most and least computationally intensive video samples processed by the C3D model. Specifically, Figures 8a and 8b display four downsampled frames from the rafting and skiing activities, respectively. The rafting sequence requires 14.5 GFLOPs for inference, whereas the skiing sequence requires approximately one-third of that computation.

Consistent with Figure 7, the rafting video’s high frame-to-frame variability and spatial detail drive higher R^s and R^t levels. Conversely, the skiing video’s uniform background and localized motion reduce spatio-temporal complexity, lowering computational demand.

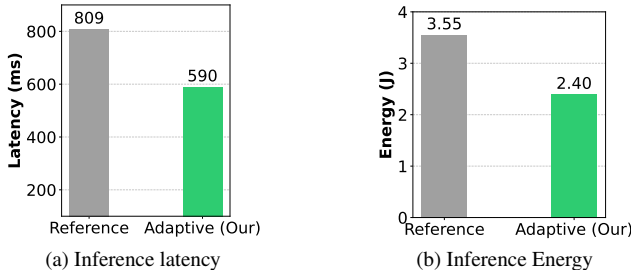


Figure 9. R(2+1)D latency and energy on Jetson Nano.

We evaluate computational efficiency on two edge architectures: an NVIDIA Jetson Nano (4GB GPU) and a Samsung S22 (Qualcomm Snapdragon 8 Gen 1 ARM CPU). To optimize platform-specific constraints—branching penalties on GPUs and vectorization capabilities on CPUs—we employ temporal/channel pruning for the GPU and temporal/spatial pruning for the CPU. GPU Implementation: We implemented R(2+1)D on the Jetson Nano using UCF101. The decomposed convolution structure of R(2+1)D is less memory-intensive, suiting the GPU’s restricted RAM. La-

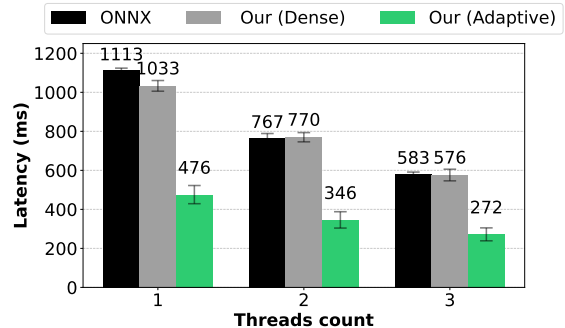


Figure 10. C3D inference latency on CPU (UCF101) vs. baseline.

tency was measured via GPU clock time, and power was recorded using an external PSU (reported as delta over idle).

As shown in Figures 9a and 9b, our adaptive method achieves a $1.37\times$ latency reduction and $1.47\times$ better energy efficiency over the PyTorch baseline. On the mobile CPU, we developed a custom C3D kernel optimized for ARMv9. We leveraged Neon SIMD instructions and FP16 (Half-Precision) to mitigate memory bottlenecks. Figure 10 compares three implementations: an ONNX baseline (with standard Conv-BN-ReLU fusions), our custom Dense kernel, and our Adaptive Pruning kernel. Across 1, 2, and 3 threads, our Dense kernel matches the ONNX baseline; however, the Adaptive Pruning method delivers a substantial $2.22\times$ average speedup. The sub-linear scaling observed with increased thread counts suggests the system is memory-bandwidth bound rather than compute-bound. This indicates that the shared memory bus saturates before the execution units, presenting an opportunity for even more aggressive pruning to further alleviate memory pressure.

7. Conclusion

We propose *DANCE*, a fine-grained activation pruning framework for 3D CNNs, enabling energy-efficient inference on edge devices. Using activation variance to guide pruning, the method adapts dynamically to input complexity. It surpasses SOTA pruning approaches in both efficiency and accuracy, even after accounting for the controller overhead. The framework generalizes across datasets and can be extended to other high-cost models such as vision transformers.

References

- [1] Shivam Aggarwal, Kuluhan Binici, and Tulika Mitra. Crisp: Hybrid structured sparsity for class-aware model pruning, 2024. 2
- [2] Yoshua Bengio, Nicholas Léonard, and Aaron Courville. Estimating or propagating gradients through stochastic neurons for conditional computation. *arXiv preprint arXiv:1308.3432*, 2013. 5
- [3] Hanting Chen, Yunhe Wang, Han Shu, Yehui Tang, Chunjing Xu, Boxin Shi, Chao Xu, Qi Tian, and Chang Xu. Frequency domain compact 3d convolutional neural networks. In *2020 IEEE/CVF Conference on Computer Vision and Pattern Recognition (CVPR)*, pages 1638–1647, 2020. 2
- [4] Zhoung Chen, Yang Li, Samy Bengio, and Si Si. You look twice: Gaternet for dynamic filter selection in cnns. In *Proceedings of the IEEE/CVF Conference on Computer Vision and Pattern Recognition*, pages 9172–9180, 2019. 1
- [5] Determine Filters’Importance. Pruning filters for efficient convnets. *arXiv preprint arXiv:1608.08710*, 2016. 1
- [6] Shangqian Gao, Yanfu Zhang, Feihu Huang, and Heng Huang. Bilevelpruning: Unified dynamic and static channel pruning for convolutional neural networks. In *2024 IEEE/CVF Conference on Computer Vision and Pattern Recognition (CVPR)*, pages 16090–16100, 2024. 2
- [7] Xitong Gao, Yiren Zhao, Robert Mullins, Chengzhong Xu, et al. Dynamic channel pruning: Feature boosting and suppression. *arXiv preprint arXiv:1810.05331*, 2018. 1
- [8] Jinyang Guo, Dong Xu, and Wanli Ouyang. Multidimensional pruning and its extension: A unified framework for model compression. *IEEE Transactions on Neural Networks and Learning Systems*, 35(9):13056–13070, 2024. 6
- [9] Yihui He, Xiangyu Zhang, and Jian Sun. Channel pruning for accelerating very deep neural networks. In *Proceedings of the IEEE international conference on computer vision*, pages 1389–1397, 2017. 1
- [10] Charles Herrmann, Richard Strong Bowen, Neal Wadhwa, Rahul Garg, Qiurui He, Jonathan T Barron, and Ramin Zabih. Learning to autofocus. In *Proceedings of the IEEE/CVF Conference on Computer Vision and Pattern Recognition*, pages 2230–2239, 2020. 7
- [11] Jian Hu, Jason Klein Liu, Haotian Xu, and Wei Shen. Reinforce++: An efficient rlhf algorithm with robustness to both prompt and reward models, 2025. 2
- [12] Weizhe Hua, Yuan Zhou, Christopher M De Sa, Zhiru Zhang, and G Edward Suh. Channel gating neural networks. *Advances in neural information processing systems*, 32, 2019. 1
- [13] Eric Jang, Shixiang Gu, and Ben Poole. Categorical reparameterization with gumbel-softmax, 2017. 2, 5
- [14] Mengnan Jiang, Jingcun Wang, Amro Eldebiky, Xunzhao Yin, Cheng Zhuo, Ing-Chao Lin, and Grace Li Zhang. Class-aware pruning for efficient neural networks, 2024. 2
- [15] Will Kay, Joao Carreira, Karen Simonyan, Brian Zhang, Chloe Hillier, Sudheendra Vijayanarasimhan, Fabio Viola, Tim Green, Trevor Back, Paul Natsev, Mustafa Suleyman, and Andrew Zisserman. The kinetics human action video dataset, 2017. 6
- [16] H. Kuehne, H. Jhuang, E. Garrote, T. Poggio, and T. Serre. Hmdb: A large video database for human motion recognition. In *2011 International Conference on Computer Vision*, pages 2556–2563, 2011. 6
- [17] Hao Li, Asim Kadav, Igor Durdanovic, Hanan Samet, and Hans Peter Graf. Pruning filters for efficient convnets, 2017. 6
- [18] Hengduo Li, Zuxuan Wu, Abhinav Shrivastava, and Larry S. Davis. 2d or not 2d? adaptive 3d convolution selection for efficient video recognition. *2021 IEEE/CVF Conference on Computer Vision and Pattern Recognition (CVPR)*, pages 6151–6160, 2020. 2
- [19] Zhuang Liu, Jianguo Li, Zhiqiang Shen, Gao Huang, Shoumeng Yan, and Changshui Zhang. Learning efficient convolutional networks through network slimming. In *Proceedings of the IEEE international conference on computer vision*, pages 2736–2744, 2017. 1
- [20] Jian-Hao Luo, Jianxin Wu, and Weiyao Lin. Thinet: A filter level pruning method for deep neural network compression. In *Proceedings of the IEEE international conference on computer vision*, pages 5058–5066, 2017. 1
- [21] Chris J. Maddison, Andriy Mnih, and Yee Whye Teh. The concrete distribution: A continuous relaxation of discrete random variables, 2017. 2, 5
- [22] Mrinal Mathur, Barak A. Pearlmutter, and Sergey M. Plis. MIND over body: Adaptive thinking using dynamic computation. In *The Thirteenth International Conference on Learning Representations*, 2025. 1
- [23] Andrzej Maćkiewicz and Waldemar Ratajczak. Principal components analysis (pca). *Computers & Geosciences*, 19(3):303–342, 1993. 3
- [24] Pavlo Molchanov, Stephen Tyree, Tero Karras, Timo Aila, and Jan Kautz. Pruning convolutional neural networks for resource efficient inference, 2017. 6
- [25] Wei Niu, Mengshu Sun, Zhengang Li, Jou-An Chen, Jiexiong Guan, Xipeng Shen, Yanzhi Wang, Sijia Liu, Xue Lin, and Bin Ren. Rt3d: Achieving real-time execution of 3d convolutional neural networks on mobile devices, 2021. 2, 6

- [26] Priyadarshini Panda, Abhronil Sengupta, and Kaushik Roy. Conditional deep learning for energy-efficient and enhanced pattern recognition. In *Proceedings of the 2016 Conference on Design, Automation & Test in Europe*, page 475–480, San Jose, CA, USA, 2016. EDA Consortium. 1, 2
- [27] Olga Russakovsky, Jia Deng, Hao Su, Jonathan Krause, Sanjeev Satheesh, Sean Ma, Zhiheng Huang, Andrej Karpathy, Aditya Khosla, Michael Bernstein, et al. Imagenet large scale visual recognition challenge. *International journal of computer vision*, 115(3):211–252, 2015. 1
- [28] Mahmoud Salem, Mohamed Osama Ahmed, Frederick Tung, and Gabriel Oliveira. Gumbel-softmax selective networks, 2022. 5
- [29] Chun-Hung Shen and Homer H Chen. Robust focus measure for low-contrast images. In *2006 Digest of technical papers international conference on consumer electronics*, pages 69–70. IEEE, 2006. 7
- [30] Khurram Soomro, Amir Zamir, and Mubarak Shah. Ucf101: A dataset of 101 human actions classes from videos in the wild. *ArXiv*, abs/1212.0402, 2012. 6
- [31] Mingxing Tan and Quoc Le. Efficientnet: Rethinking model scaling for convolutional neural networks. In *International conference on machine learning*, pages 6105–6114. PMLR, 2019. 1
- [32] Du Tran, Lubomir Bourdev, Rob Fergus, Lorenzo Torresani, and Manohar Paluri. Learning spatiotemporal features with 3d convolutional networks, 2015. 6
- [33] Du Tran, Lubomir Bourdev, Rob Fergus, Lorenzo Torresani, and Manohar Paluri. Learning spatiotemporal features with 3d convolutional networks. In *Proceedings of the IEEE international conference on computer vision*, pages 4489–4497, 2015. 1
- [34] Du Tran, Heng Wang, Lorenzo Torresani, Jamie Ray, Yann LeCun, and Manohar Paluri. A closer look at spatiotemporal convolutions for action recognition, 2018. 6
- [35] Xin Wang, Fisher Yu, Zi-Yi Dou, Trevor Darrell, and Joseph E. Gonzalez. Skipnet: Learning dynamic routing in convolutional networks, 2018. 1, 2
- [36] Ronald J Williams. Simple statistical gradient-following algorithms for connectionist reinforcement learning. *Machine Learning*, 8:229–256, 1992. 2
- [37] Sanghyun Woo, Jongchan Park, Joon-Young Lee, and In So Kweon. Cbam: Convolutional block attention module. In *Computer Vision – ECCV 2018: 15th European Conference, Munich, Germany, September 8–14, 2018, Proceedings, Part VII*, page 3–19, Berlin, Heidelberg, 2018. Springer-Verlag. 3
- [38] Wenxuan Wu, Zhongang Qi, and Li Fuxin. Pointconv: Deep convolutional networks on 3d point clouds. In *2019 IEEE/CVF Conference on Computer Vision and Pattern Recognition (CVPR)*, pages 9613–9622, 2019. 1
- [39] Zuxuan Wu, Tushar Nagarajan, Abhishek Kumar, Steven Rennie, Larry S. Davis, Kristen Grauman, and Rogerio Feris. Blockdrop: Dynamic inference paths in residual networks, 2019. 2
- [40] Wenhan Xia, Hongxu Yin, Xiaoliang Dai, and Niraj Kumar Jha. Fully dynamic inference with deep neural networks. *IEEE Transactions on Emerging Topics in Computing*, 10:962–972, 2020. 1, 2
- [41] Zhiwei Xu, Thalaiyasingam Ajanthan, Vibhav Vineet, and Richard Hartley. Ranp: Resource aware neuron pruning at initialization for 3d cnns, 2021. 2
- [42] Huanrui Yang, Wei Wen, and Hai Li. Deepfayer: Learning sparser neural network with differentiable scale-invariant sparsity measures. *arXiv preprint arXiv:1908.09979*, 2019. 4
- [43] Chenxin Zhang, Keqin Xu, Jie Liu, Zhiyang Zhou, Liangyi Kang, and Dan Ye. Identity-linked group channel pruning for deep neural networks. In *2021 International Joint Conference on Neural Networks (IJCNN)*, pages 1–9, 2021. 6
- [44] Junzi Zhang, Jongho Kim, Brendan O’Donoghue, and Stephen Boyd. Sample efficient reinforcement learning with reinforce, 2020. 2